The Astrophysical Journal, 588:L45–L48, 2003 May 1

A THREE-DIMENSIONAL FLUX ROPE MODEL FOR CORONAL MASS EJECTIONS BASED ON A LOSS OF EQUILIBRIUM

Ilia I. Roussev,[1] Terry G. Forbes,[2] Tamas I. Gombosi,[1] Igor V. Sokolov,[1] Darren L. DeZeeuw,[1] and Joachim Birn[3]
Received 2003 February 4; accepted 2003 March 21; published 2003 March 28

ABSTRACT

A series of simulation runs are carried out to investigate the loss of equilibrium of the three-dimensional flux rope configuration of Titov & Démoulin as a suitable mechanism for the initiation of coronal mass ejections. By means of these simulations, we are able to determine the conditions for which stable equilibria no longer exist. Our results imply that it is possible to achieve a loss of equilibrium even though the ends of the flux rope are anchored to the solar surface. However, in order to have the flux rope escape, it is necessary to modify the configuration by eliminating the arcade field.

Subject headings: MHD — Sun: corona — Sun: coronal mass ejections (CMEs) — Sun: flares — Sun: magnetic fields

1. INTRODUCTION

The numerical simulations presented in this Letter were designed to test an analytical model for the initiation of coronal mass ejections (CMEs) developed by Titov & Démoulin (1999, hereafter T&D). Their model is derived from a long line of previous analytical models containing flux ropes suspended in the corona by a balance between magnetic compression and tension forces (see the reviews by Forbes 2000 and Low 2001). In the two-dimensional models, a flux rope with current I has two possible equilibrium positions, provided that the current is not too large. The one closest to the Sun is stable, but the one farthest from the Sun is unstable. As the current in the flux rope increases, the two equilibrium locations approach one another, and they meet when the current reaches a critical value. There are no equilibria for flux ropes with current above this value. The difference in the stability properties of the two equilibria comes from the fact that one sits in a magnetic energy valley while the other one sits on a hill. In other words, for the unstable equilibria, a small outward displacement of the flux rope leads to an outward force, which acts to increase the displacement.

The T&D model uses a fully three-dimensional magnetic field configuration that is remarkably realistic looking when compared with observations, but until now there has been no rigorous test to determine whether the model can produce an eruption. Previous two-dimensional MHD models (e.g., Forbes & Priest 1995), whose eruptive properties are well established, both analytically (Forbes & Isenberg 1991) and numerically (Forbes 1990, 1991), suggest that an eruption will occur provided that the anchoring of the ends of the flux rope to the solar surface does not prevent it (Antiochos, DeVore, & Klimchuk 1999).

More recently, Amari et al. (2000) and Linker et al. (2001) have carried out simulations that are closely related to the model of T&D. In these simulations, a flux rope is formed by first shearing an arcade and then subsequently pushing the opposite polarity feet of the arcade toward one another and allowing them to reconnect. Continued reconnection of the feet weakens the ability of the overlying, unreconnected field lines of the arcade to hold the flux rope next to the surface, and eventually the flux rope erupts. In a numerical simulation with continually evolving boundary conditions, some care needs to be taken to determine whether the subsequent evolution is really due to a loss of equilibrium or simply a consequence of driving by the boundary conditions.

One way to test the equilibrium properties of a configuration is to evolve the boundary conditions very slowly until it erupts (Linker et al. 2001). Here, we choose a different approach by taking advantage of the fact that our initial configuration is derived from an analytical model for which the equilibria locations are known. We start with an initial condition that is at rest, and we use a nonevolving boundary condition so that no kinetic energy is fed into the system either from the initial state or from the boundaries. Thus, any dynamical evolution that is observed must result from the fact that the initial state is not in a stable equilibrium.

2. NUMERICAL FORMULATION

The T&D model consists of a circular flux rope that is embedded in a line-tying surface as shown in Figure 1. The hoop force of the rope (see Shafranov 1966) is counterbalanced by the field from two point magnetic charges buried at a depth $z = -d$ below the surface and located at $x = \pm L$. In addition to the external field generated by the point charges, the model allows a contribution from an infinitely long line current, I_0, that coincides with the x-axis and also lies below the photosphere at depth d (not shown in Fig. 1).

The purpose of the toroidal field produced by the imaginary line current below the surface is to reduce the number of turns of the field lines within and outside the flux rope. Without the line current, the field lines at the surface of the flux rope are purely poloidal, and they have an infinite number of turns in a finite length. However, some observations (Leroy, Bommier, & Sahal-Brechot 1983; Gaizauskas 1979) imply that the maximum number of turns is less than two, but these observations do not include the cavity region that may comprise most of the flux rope. Incorporating the line current eliminates this problem by creating a toroidal field that ensures that no field lines are highly twisted. By adjusting the strength of the line current, one can achieve a reasonable amount of twist everywhere.

T&D have also considered the stability of their configuration and found that it may be unstable if the large radius, R, of the flux rope exceeds $\sqrt{2}L$, where L is half the distance between the

[1] Center for Space Environment Modeling, University of Michigan at Ann Arbor, 2455 Hayward Street, Ann Arbor, MI 48109-2143; iroussev@umich.edu, tamas@umich.edu, igorsok@umich.edu, darrens@umich.edu.

[2] Department of Physics, Demeritt, Hall, and Institute for the Study of Earth, Ocean, and Space, University of New Hampshire, Durham, NH 03824; terry.forbes@unh.edu.

[3] Los Alamos National Laboratory, NIS-1, P.O. Box 1663, Los Alamos, NM 87545; jbirn@lanl.gov.

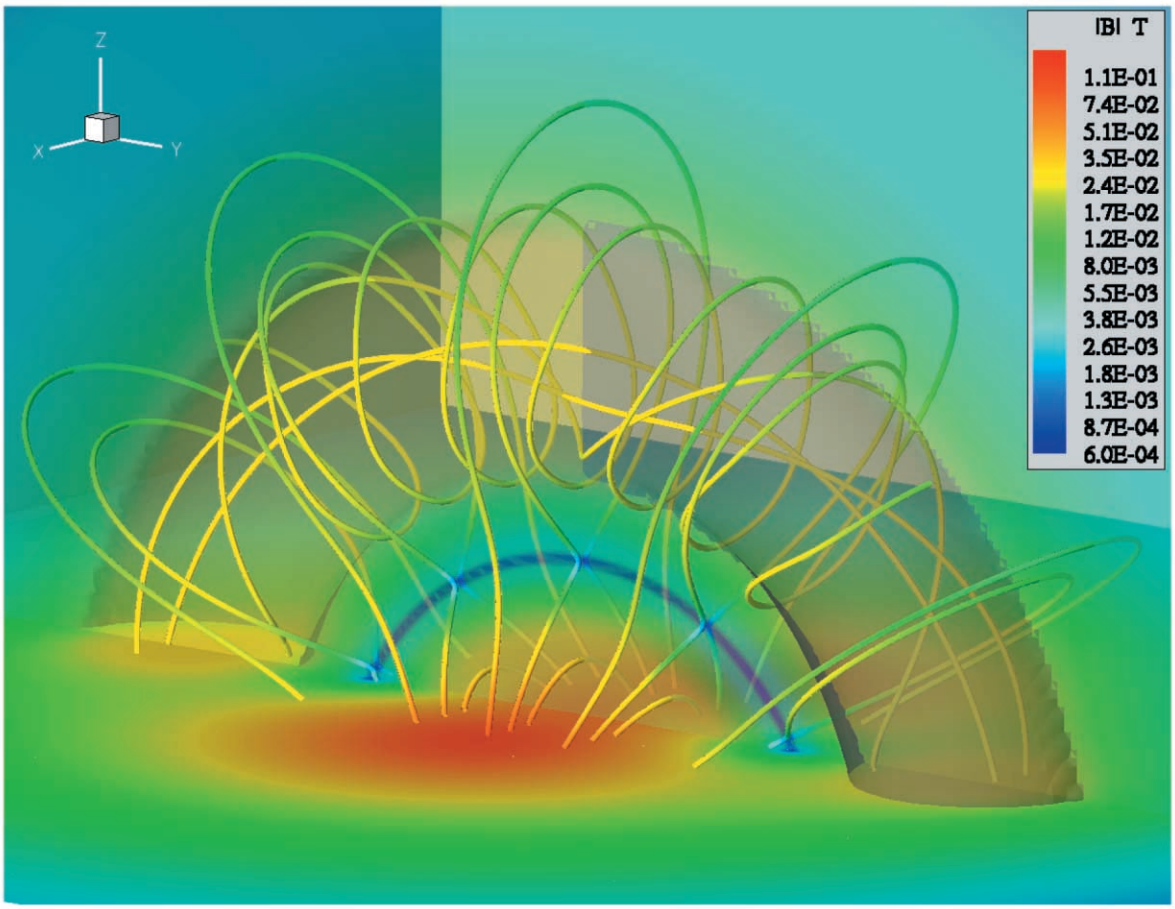

FIG. 1.—Three-dimensional view of the magnetic field configuration for the initial state. The solid lines are magnetic field lines, where the false-color code visualizes the magnetic field strength in units of tesla. The surface shaded in gray is an isosurface of $B_z = 0$.

background sources $\pm q$. This is only a necessary condition for instability because their analysis does not include the effects of the line-tying of the poloidal field circulating around the flux rope.

In our simulations, the background atmosphere is constructed by solving the static momentum equation with a prescribed temperature variation with height (measured along z in our notation). In the force-free limit, the kinetic gas pressure, p, is obtained from $dp/dz = -\rho g$, while the mass density, ρ, is derived from the perfect gas law. We assign a constant value of gravity acceleration of $g = 274.1$ m s^{-2}, and all thermodynamic variables are assumed uniform in the horizontal plane. The plasma temperature increases from a value of 5.1×10^3 K at the photosphere to a coronal value of 1.02×10^6 K, across a narrow transition region of 6.144×10^6 m, as prescribed by the formula $T = 1 + 99.5\ \{1 + \tanh [0.1\ (z - 70)]\}$. The sound speed at the photosphere is 6.488×10^3 m s^{-1}, and the characteristic value of mass density is chosen as 2.7×10^{-6} kg m^{-3}.

The flux rope initially has a major radius $R = 1.0 \times 10^8$ m, a minor radius $a = 0.2R$, and the strength of the two subphotospheric sources, q, is 10^{14} T m^2. The sources are located at $d = 2.0 \times 10^7$ m, and $L = 0.3R$. With the above choice of parameters, the equilibrium toroidal current flowing inside the flux rope is 2.293×10^{12} A, and it has a uniform distribution over the volume. As we will discuss in § 3, we find that it is necessary to set I_0 to zero in order for the flux rope to escape.

The full set of ideal MHD equations, in conservative form, are solved using the Block Adaptive Tree Solar Wind Roe-type Upwind Scheme (BATS-R-US) code (Powell et al. 1999; Groth et al. 2000), in a combination with the Artificial Wind approximate Riemann solver (Sokolov et al. 2002). This numerical solver uses a finite volume second-order scheme based on upwind differencing combined with a limited linear reconstruction algorithm. The MHD solution is advanced in time using an explicit time-stepping algorithm. The BATS-R-US code is designed to run efficiently on massively parallel computers and solves the MHD equations with the use of block adaptive mesh refinement (AMR). We use a simplified energy equation that neglects the effects of radiative losses, heat conduction, and background heating. The dissipative effects due to viscosity and electric resistivity are not treated explicitly, but the numerical scheme provides some finite numerical dissipation where needed, for example, in the current sheets and shocks. The solenoidal constraint is treated using an eight-wave scheme (Powell et al. 1999), meaning that additional terms are added to the equations to prevent any accumulation of errors in the condition that $\nabla \cdot B = 0$.

The simulation region is a cube with a length of 400 Mm, and the numerical grid is chosen to be nonuniform. In the simulations we discuss here, AMR was not activated in order to allow us to do a larger number of runs at reduced costs. The total number of cells within the numerical domain is 7,281,408. We applied six levels of torus-focused initial refinement,[4] with the intent to assign the highest spatial resolution at the region of the flux rope and at the photosphere-corona transition layer.

[4] There is a factor of 2 difference in spatial resolution at each refinement level change.

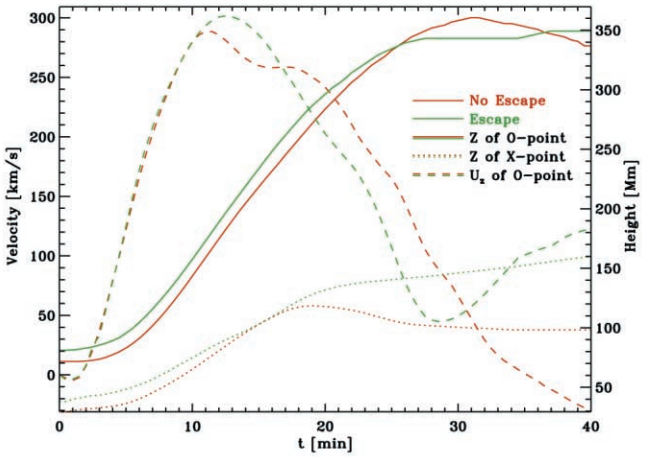

FIG. 2.—Height vs. time curves for the O-point (*solid curve*) and the X-point (*dotted curve*). The vertical velocity of the O-point vs. time is shown as the dashed curve. The escape case is shown in green, whereas the no-escape case appears in red.

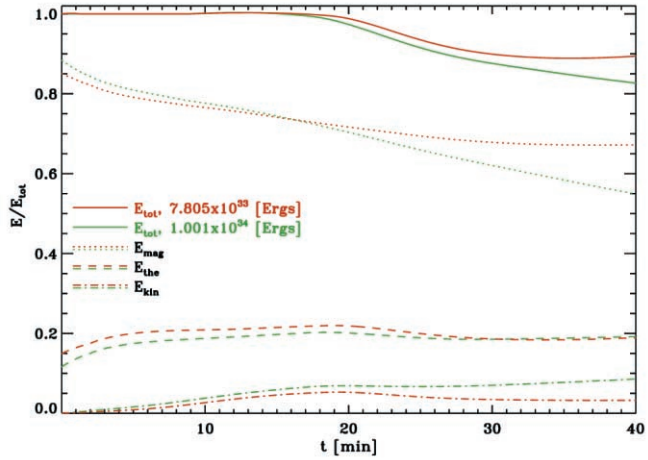

FIG. 3.—Curves of the total (*solid curve*), magnetic (*dotted curve*), thermal (*dashed curve*), and kinetic energy (*dash-dotted curve*), in units of 10^{34} ergs, vs. time for the whole duration of the simulation.

The underlying motivation was to keep the discretization errors small during the initialization of the physical variables, to start with an initial state as close to equilibrium as possible.

The boundary conditions consist of an impenetrable and highly conducting bottom boundary (at $z = 0$); outflow side boundaries (at $x = \pm 200$ Mm and $y = \pm 200$ Mm); and an open top boundary (at $z = 400$ Mm). At the bottom boundary of the numerical domain, the velocity components are maintained at zero throughout the simulation runs, and the normal component of the magnetic field is fixed and set to its value at $t = 0$. This way, we ensure that there is no energy flux through the boundary. Floating (zero gradient) conditions are applied to the tangential components of the magnetic field and mass density. The gas pressure in the ghost cells is obtained from $dp = -\rho g\, dz$. The open boundary conditions are implemented by applying a floating condition to all physical variables. The side boundaries are the same as the top boundary, except that any inflow is prevented.

By adding a photosphere-corona transition layer, the bottom boundary of the numerical domain lies well below the physical boundary corresponding to the photosphere. Thus, the line-tying of the field is implemented within the numerical domain rather than at the numerical boundary (see Karpen, Antiochos, & DeVore 1991). This allows the surface currents associated with the line-tying to be included in the simulations.

3. DYNAMICAL EVOLUTION

Flux ropes having a small number of turns (~1–4) did not manifest any loss of equilibrium, but highly twisted ones (~200) did. However, the resulting evolution of the system more closely resembled an impulsive-type flare rather than a CME-like event because the flux rope did not escape but instead came to a stop. This is because of the overall dominance at high altitudes of the static arcade field produced by the subsurface line current. Therefore, to have flux ropes that could escape, we had to remove the arcade field by setting the subphotospheric line current to zero. With this modification, the flux rope does escape, but the number of turns in the field lines at the surface of the flux rope approaches infinity as the distance from the axis increases to a (see Fig. 1).

The approximate analytical formulae (i.e., they assume $a/R \ll 1$) used to construct the initial state and the discretization errors lead to a small initial disturbance. This causes the flux rope to drift downward for just a couple of minutes until the restoring force due to the compression of the field reverses the direction.

After the initial adjustment, the flux rope undergoes an increase in acceleration. As seen in Figure 2, the slope of the speed curve for the O-point is initially shallow, just as expected for a loss of equilibrium (Lin & Forbes 2000). The upward motion of the rope eventually leads to the formation of a current sheet at the location of the preexisting X-line. Once the current sheet starts forming, the flux rope begins to decelerate. The effects of the line-tying at the ends of the flux rope may also contribute to this deceleration. Another effect that we see at this time (which is an entirely three-dimensional effect) is that most of the magnetic helicity has been transported by torsional Alfvén waves from the footprints of the flux rope toward its top. As a result, the restraining effect caused by the line-tying of the feet of the flux rope becomes important.

The energetics of the eruption are presented in Figure 3. For the escape case, at the beginning of the simulation, the thermal, magnetic, kinetic, and gravitational energies are, respectively, 13%, 87%, 0%, and 10% of the total energy. This reflects the initial dominance of the magnetic energy over all other forms. At $t \approx 19$ minutes, when the first outflow through the numerical boundaries starts to occur, these energy ratios are 21% (thermal), 72% (magnetic), 7% (kinetic), and 10% (gravitational). Thus, about 17% of the initial magnetic energy has been converted into nearly equal amounts of kinetic and thermal energy. The amount of kinetic energy, summed over the whole computational domain, toward the end of the experiment is of the order of 10^{33} ergs. The change in gravitational energy is less than 2% over the whole simulation.

A three-dimensional view of the magnetic field configuration at $t = 35$ minutes is shown in Figure 4. A close look at the footprints of the rope reveals closed loops connecting the two flux regions, namely, the flux rope region and the $\pm q$ sources at $x = \pm L$. The most plausible explanation of this structure is that there is an interchange reconnection between the highly twisted field lines of the flux rope and the overlying closed field lines from the $\pm q$ sources. As a result of this process, the newly created closed field lines connect the two flux regions. The isosurface of $B_z = 0$ shown in Figure 1 (*shaded in gray*) indicates where this process preferentially takes place.

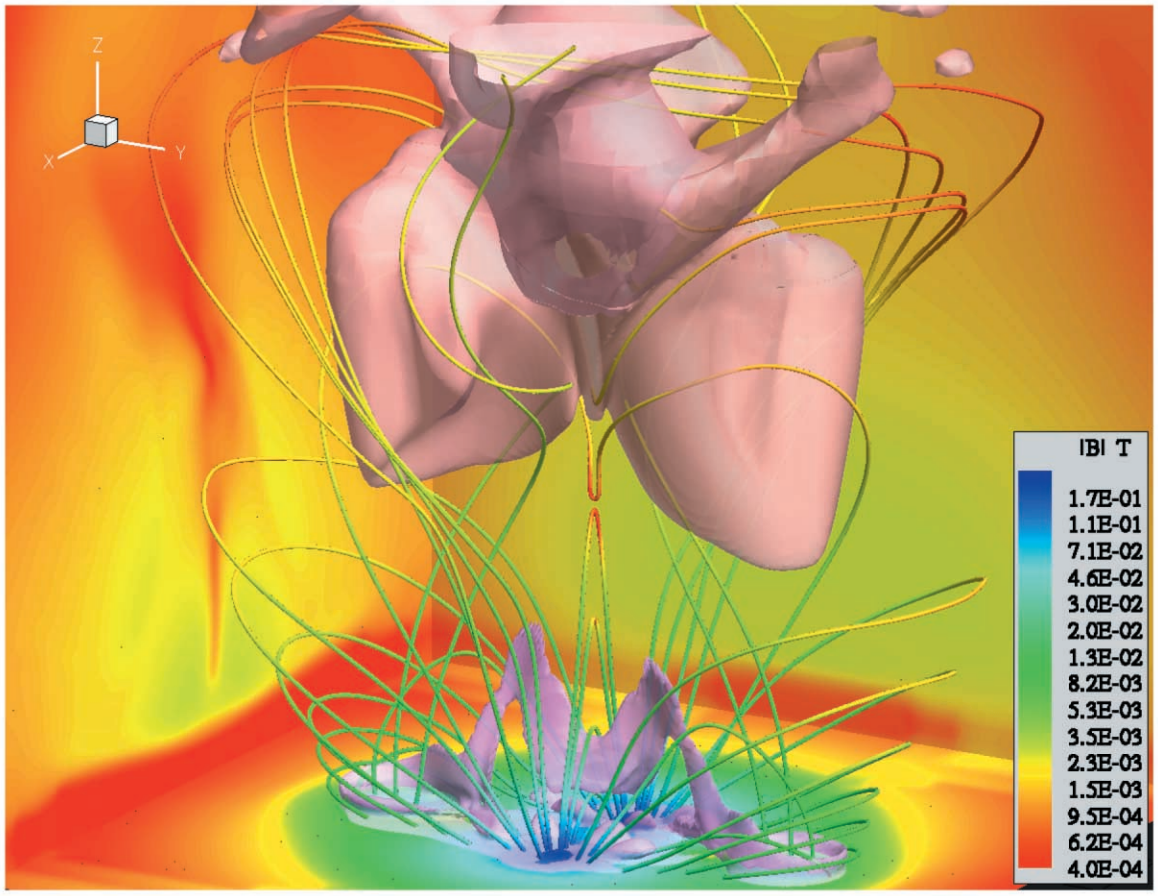

FIG. 4.—Three-dimensional view of the magnetic field configuration at $t = 35$ minutes. As in Fig. 1, the solid lines are magnetic field lines. The false color shows the magnetic field strength. The lower surface, shaded in purple, is an isosurface of electric current density of magnitude 0.0015 A m^{-2}. The upper surface, shaded in maroon, is an isosurface of flow velocity of magnitude 200 km s^{-1}.

4. CONCLUSIONS

Our results show that the criterion $R > \sqrt{2}L$, derived in the T&D model by neglecting the effects of line-tying of the poloidal field, may be a necessary condition for an eruption, but it is not a sufficient one. We find that larger values of R in excess of 5 are required.

We also find that even when the initial equilibrium is unstable, the flux rope cannot escape, unless the static arcade field associated with the line current is removed. Thus, although the T&D model can produce a CME-like eruption, it cannot do so without requiring a highly twisted field at the surface of the flux rope. It may be possible in the future to mitigate this by using a configuration in which the infinitely long line current is replaced by a current source whose magnetic field falls off more rapidly with height.

Magnetic reconnection plays a crucial role in dissipating the current sheet, thus helping the flux rope eruption to proceed. In future investigations, a more realistic treatment of the reconnection process in the current sheet and the incorporation of a spherical geometry may greatly reduce the deceleration that we observe in our modified T&D configuration.

The authors thank S. K. Antiochos, B. C. Low, and an unknown referee for their comments. This research work was supported by DoD MURI grant F49620-01-1-0359, NSF CISE grant ACI-9876943, NASA AISRP grant NAG5-9406 at the University of Michigan, as well as NASA grants NAG5-8228, 10977, and 10852.

REFERENCES

Amari, T., Luciani, J. F., Mikić, Z., & Linker, J. 2000, ApJ, 529, L49
Antiochos, S. K., DeVore, C. R., & Klimchuk, J. A. 1999, ApJ, 510, 485
Forbes, T. G. 1990, J. Geophys. Res., 95, 11,919
———. 1991, Geophys. Astrophys. Fluid Dyn., 62, 16
———. 2000, J. Geophys. Res., 105, 23,153
Forbes, T. G., & Isenberg, P. A. 1991, ApJ, 373, 294
Forbes, T. G., & Priest, E. R. 1995, ApJ, 446, 377
Gaizauskas, V. 1979, in IAU Colloq. 44, Physics of Solar Prominences, ed. E. Jensen, P. Maltby, & F. Q. Orrall (Oslo: Oslo Univ. Press), 272
Groth, C. P. T., DeZeeuw, D. L., Gombosi, T. I., & Powell, K. G. 2000, J. Geophys. Res., 105, 25,053
Karpen, J. T., Antiochos, S. K., & DeVore, C. R. 1991, ApJ, 382, 327
Leroy, J. L., Bommier, V., & Sahal-Brechot, S. 1983, Sol. Phys., 83, 135
Lin, J., & Forbes, T. G. 2000, J. Geophys. Res., 105, 2375
Linker, J., Lionello, R., Mikić, Z., & Amari, T. 2001, J. Geophys. Res., 106, 25,165
Low, B. C. 2001, J. Geophys. Res., 106, 25,141
Powell, K. G., Roe, P. L., Linde, T. J., Gombosi, T. I., & DeZeeuw, D. L. 1999, J. Comput. Phys., 154, 284
Shafranov, V. D. 1966, Rev. Plasma Phys., 2, 103
Sokolov, I. V., Timofeev, E. V., Sakai, J. I., & Takayama, K. 2002, J. Comput. Phys., 181, 354
Titov, V. S., & Démoulin, P. 1999, A&A, 351, 707 (T&D)